

Mechanisms of Andreev reflection in quantum Hall graphene

Antonio L. R. Manesco^{1,2,*}, Ian Matthias Flór², Chun-Xiao Liu^{2,3}, Anton R. Akhmerov²

¹ Computational Materials Science Group (ComputEEL), Escola de Engenharia de Lorena, Universidade de São Paulo (EEL-USP), Materials Engineering Department (Demar), Lorena – SP, Brazil

² Kavli Institute of Nanoscience, Delft University of Technology, Delft 2600 GA, The Netherlands

³ Qutech, Delft University of Technology, Delft 2600 GA, The Netherlands.

* am@antonioManesco.org

March 1, 2025

Abstract

We simulate a hybrid superconductor-graphene device in the quantum Hall regime to identify the origin of downstream resistance oscillations in a recent experiment [Zhao *et al.* [Nature Physics](#) **16**, (2020)]. In addition to the previously studied Mach-Zehnder interference between the valley-polarized edge states, we consider disorder-induced scattering, and the previously overlooked appearance of the counter-propagating states generated by the interface density mismatch. Comparing our results with the experiment, we conclude that the observed oscillations are induced by the interfacial disorder, and that lattice-matched superconductors are necessary to observe the alternative ballistic effects.

Contents

1	Introduction	2
2	Andreev interference in clean graphene quantum Hall devices	3
3	Effect of disorder	5
4	Effects of Fermi level mismatch	5
5	Experimental relevance	7
6	Conclusion	8
A	Valley-dependence of Andreev reflection in quantum Hall graphene	9
B	Low-energy model derivation	10
C	Absorption of quasi-particle excitations by the superconductor	13

1 Introduction

Already since the early years of graphene, researchers were able to fabricate and measure high-quality graphene–superconductor devices [1, 2]. The ease of fabrication inspired a plethora of works examining tunneling spectroscopy [3, 4], Josephson effect [2, 5–7], multiple Andreev reflections [8], imaging Andreev scattering, [9] quantum phase transitions [10, 11], reflectionless tunneling [12], microwave circuits [13], and bolometer devices [14] as well as other physical phenomena. Because quantum Hall effect in graphene manifests already at relatively low magnetic fields below 1 T, graphene is also uniquely fit to combine quantum Hall physics with superconductivity and Andreev reflection [15–18].

A recent work observed a strongly fluctuating downstream resistance in a multiterminal device as a function of the magnetic field and the gate voltage, shown in Fig 1(b). The authors have interpreted the data as chiral Andreev edge states interference, supported by tight-binding calculations [16]. This finding contradicts the idealized theory [19] that predicts that Andreev conductance of graphene in the lowest quantum Hall plateau should be constant. This feature is a consequence of three factors combined. First, the boundary conditions imposed by generic graphene terminations ensure valley number conservation and also favor the population of one sublattice [20, 21]. Second, the lowest Landau level states are valley-sublattice locked [20, 22], resulting in valley-polarized quantum Hall edge states. Finally, at the interface with a superconductor, electron edge states hybridize with hole states with opposite valley isospin and the resulting chiral Andreev edge states generate a nonlocal transport signal. Hence, conductance depends solely on device geometry (see App. A for details) [19]. In particular, if the two edges connected to the superconductor are parallel, as depicted in Fig. 1(a), the conductance between the two normal leads equals

$$G_{xx} = -\frac{2e^2}{h}, \quad (1)$$

where e is the electron charge and h is the Planck constant [19].

Our goal is to investigate Andreev states’ interference and identify its possible origins. We identify three mechanisms leading to deviations from constant conductance. The first option, proposed in Ref. [16], is the Andreev interference created by the lattice mismatch (Sec. 2). We find that most interface orientations lead to vanishing Andreev interference due to the suppressed intervalley coupling. Turning to another possibility, the short-range disorder (Sec. 3), we confirm that the large momentum transfer results in irregular oscillations between normal and Andreev reflections at any interface orientation. Finally, a sufficiently high Fermi level mismatch (Sec. 4) generates additional edge states and leads to interference through intravalley scattering.

All three mechanisms produce conductance fluctuations, albeit with different characteristics. Lattice and Fermi level mismatch at perfect interfaces generate a regular interference pattern in nonlocal conductance due to the translational invariance of the Hamiltonian. An irregular interference pattern, similar to the experimental data, occurs only in the presence of a strong

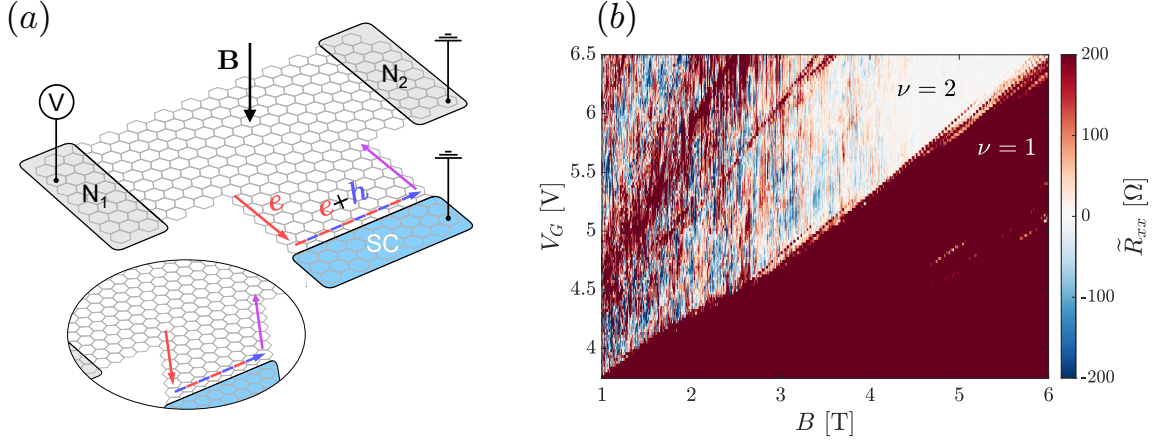


Figure 1: (a) An example device for probing nonlocal Andreev reflection in graphene. The device has 3-terminals: two normal leads (grey) and a superconducting lead (blue). Both graphene edges connected with the superconducting lead are zigzag, which mimics the valley polarization of a generic graphene boundary. The interface can be either armchair (main figure) or zigzag (inset). (b) The measured downstream resistance \tilde{R}_{xx} as a function of the magnetic field B and the gate voltage V_G in a multi-terminal setup (courtesy of Zhao *et al.* [16]). The separation between filling factors $\nu = 1$ and $\nu = 2$ is highlighted.

disorder. We compare the results with experimental data and discuss the relevance of our findings in Sec. 5.

2 Andreev interference in clean graphene quantum Hall devices

The NS interface hosts two propagating Andreev states moving along a single direction (throughout the manuscript we treat spin as a trivial degeneracy). Linearizing the dispersion of the two edge states near zero energy we obtain the edge state Hamiltonian

$$H_{\text{eff}} = \begin{pmatrix} v(k + k_0) & 0 \\ 0 & v(k - k_0) \end{pmatrix} = vk\sigma_0 + vk_0\sigma_z, \quad (2)$$

where k is the momentum along the interface, and v is the Fermi velocity of the propagating chiral modes (see App. B for a derivation). The projections of the valley momenta on the graphene-superconductor interface $\pm k_0$ depend on the lattice orientation: $k_0 \approx 0$ if the interface is along the armchair direction, while a general boundary orientation results in $k_0 \sim \pi/a$, with a the graphene lattice constant. The Hamiltonian acts on $\Psi = (\psi_1, \psi_2)^T$, where ψ_1 is a linear combination of electron states at valley K and hole states at the valley K' , and ψ_2 is the opposite. The Pauli matrices σ_0 and σ_i (with $i \in \{x, y, z\}$) act on Ψ .

Intervalley coupling

$$H_{\text{intervalley}} = m\sigma_x, \quad (3)$$

with m the coupling constant leads to Mach-Zehnder interference as a function of the magnetic field and the gate voltage [16]. A sufficiently low value of $m \ll vk_0$ preserves the valley polarization and leads to a low visibility of the interference pattern. Because the intervalley coupling is a low-energy phenomenon, we estimate $m \sim vk_F$, with k_F the Fermi momentum in graphene. Therefore intervalley coupling is non-negligible only if $k_0 \lesssim k_F$, and the conductance oscillations at an ideal interface should be visible only if the NS boundary is oriented within angles $\lesssim k_F a \sim 1^\circ$ from the armchair direction.

To confirm the absence of interference at clean NS interfaces with generic orientation (small m), we perform tight-binding calculations using the Kwant package [23]. The Hamiltonian reads

$$\mathcal{H} = \sum_i \psi_i^\dagger (\Delta_i \tau_x - \mu_i \tau_z) \psi_i - \sum_{\langle i,j \rangle} \psi_i^\dagger (t_{ij} e^{i\tau_z \phi_{ij}} \tau_z) \psi_j, \quad (4)$$

where $\psi_i = (c_i, c_i^\dagger)^T$, c_i^\dagger and c_i are the electron creation and annihilation operators at the position \mathbf{r}_i , and $\langle i, j \rangle$ are all the pairs of nearest neighbor sites. We simulate the interface by using the following position dependence of the chemical potential μ_i and the superconducting pairing potential Δ_i :

$$\mu_i = (\mu_{SC} - \mu_{QH}) f(\mathbf{r}_i) + \mu_{QH}, \quad \Delta_i = \Delta \Theta(x_i), \quad f(\mathbf{r}_i) = \frac{1}{2} \left[1 + \tanh \left(\frac{x_i}{\chi} \right) \right], \quad (5)$$

with μ_{QH} and μ_{SC} the onsite energies at the normal and the superconducting region. The hopping energies $t_{ij} = t$ are constant in the honeycomb crystal structure, and equal to $t_{ij} = t/2$ in the square lattice that we use to simulate a lattice mismatch with the superconductor. The Peierls phase is:

$$\phi_{ij} = -\frac{\pi B}{\phi_0} (y_j - y_i)(x_j + x_i) \Theta \left(\frac{x_i + x_j}{2} \right), \quad (6)$$

where B is the orbital magnetic field, $\phi_0 = h/e$ is the magnetic flux quantum, and $\Theta(x)$ is the Heaviside step function. The model is rescaled as $a \mapsto \tilde{a} = sa$ and $t \mapsto \tilde{t} = t/s$ to reduce the computational cost keeping the Fermi velocity $v_F \propto ta$ unchanged [24]. In all transport calculations, we use $t = 2.8 \text{ eV}$, $a = 0.142 \text{ nm}$ [25], $s = 10$, $\Delta = 1.3 \text{ meV}$ in order to match the MoRe pairing potential [16], and we choose $\chi = 50 \text{ nm}$ to match in order of magnitude the electrostatic estimations of a similar system [26]. In this section, we follow [16] and use a superconductor with a square lattice, which weakly breaks valley conservation. On the other hand, we use a honeycomb superconductor to perform transport calculations in the Sections 3 and 4 to remove effects of valley-mixing due to lattice mismatch. In band structure calculations, we use a larger value of $\Delta = 0.05t$ in order to demonstrate more clearly the dispersion relation of the Andreev states. The τ_i Pauli matrices, in the usual representation, act on electron-hole spinor components.

We compute conductance using a 3-terminal device with the NS interface oriented either along armchair or zigzag direction, as shown in Fig. 1(a). In both cases, the two edges adjacent to the NS interface are zigzag-type in order to mimic the valley-polarizing behavior of a generic lattice termination boundary. The conductance between the two normal leads equals

$$G_{xx} = \frac{e^2}{h} \sum_{i,j} \left(T_{ee}^{ij} - T_{he}^{ij} \right), \quad (7)$$

where T_{ee}^{ij} is the probability of an electron from channel j in the source lead N_1 to transmit as an electron to the channel i in the drain lead N_2 , and T_{he}^{ij} is the probability of an electron to transmit as a hole.

We show the band structures of the NS interface and the corresponding conductances in Fig. 2. If the NS boundary is parallel to the armchair orientation [Fig. 2(a)], the conductance shows an interference pattern [Fig. 2(c)]. Chiral modes at zigzag interfaces, on the other hand [Fig. 2(b)], have constant nonlocal conductance [Fig. 2(d)], in agreement with the analytical model. We therefore confirm that the interference of chiral Andreev states at an ideal interface is highly sensitive to its orientation. Moreover, in the generic case we expect the NS conductance to be nearly constant [19]. Since the experiment [16] did not control the lattice orientation down to the required 1° precision, we turn to alternative phenomena that can explain the observed oscillations of the downstream resistance.

3 Effect of disorder

To increase the transition rate between the two chiral states, we add short-range disorder modeled as a uniformly-distributed uncorrelated onsite potential:

$$\mathcal{H}_{\text{disorder}} = \sum_{i \in \text{edge}} \psi_i^\dagger \delta\mu_i^{(\text{edge})} \tau_z \psi_i + \sum_{i \in \text{SC}} \psi_i^\dagger \delta\mu_i^{(\text{SC})} \tau_z \psi_i, \quad (8)$$

with $\delta\mu_i^{(\text{edge})}, \delta\mu_i^{(\text{SC})} \in [-t, t]$, illustrated in Fig. 3(a). We consider two relevant types of disorder. To simulate the disorder at the edge of graphene, we apply the disorder potential ($\delta\mu_i^{(\text{edge})}$) within 6 nm from the graphene edges adjacent to the NS interface. Because this disorder extends into the bulk over a length smaller than the magnetic length $l_B = \sqrt{\hbar/eB}$, it does not introduce additional conduction channels, but it breaks the valley polarization of the edge states. Furthermore, in order to approximate the effect of coupling to a strongly disordered MoRe superconductor [16], we add $\delta\mu_i^{(\text{SC})}$ in the superconducting region ($x > 0$).

We observe that conductance in the presence of edge disorder varies only slowly [Fig. 3(b)] because the edge states near the NS interface still maintain a definite valley polarization, and the propagation along the NS interface preserves valley isospin. On the other hand, scattering caused by disorder in the superconducting region leads to strong irregular oscillations (Eq. 1) at all values of μ_{QH} and B [Fig. 3(c)].

4 Effects of Fermi level mismatch

Due to a work function difference, the superconductor dopes the graphene layer near the NS interface. According to electrostatic simulations, the region with increased charge carrier density extends over tens of nanometers [26]. However, due to its smooth potential profile, it preserves valley polarization. The potential mismatch does not qualitatively change most of the proximity physics in graphene, and therefore the potential profile is frequently approximated by a step function, as done *e. g.* in Refs. [6, 27].

We observe that in quantum Hall regime, the doping by the superconducting contact increases the filling factor near the NS interface. This introduces additional counterpropagating bands at the Fermi energy, shown in Figs. 4(a), and therefore Eq. 2 does not hold. Because the

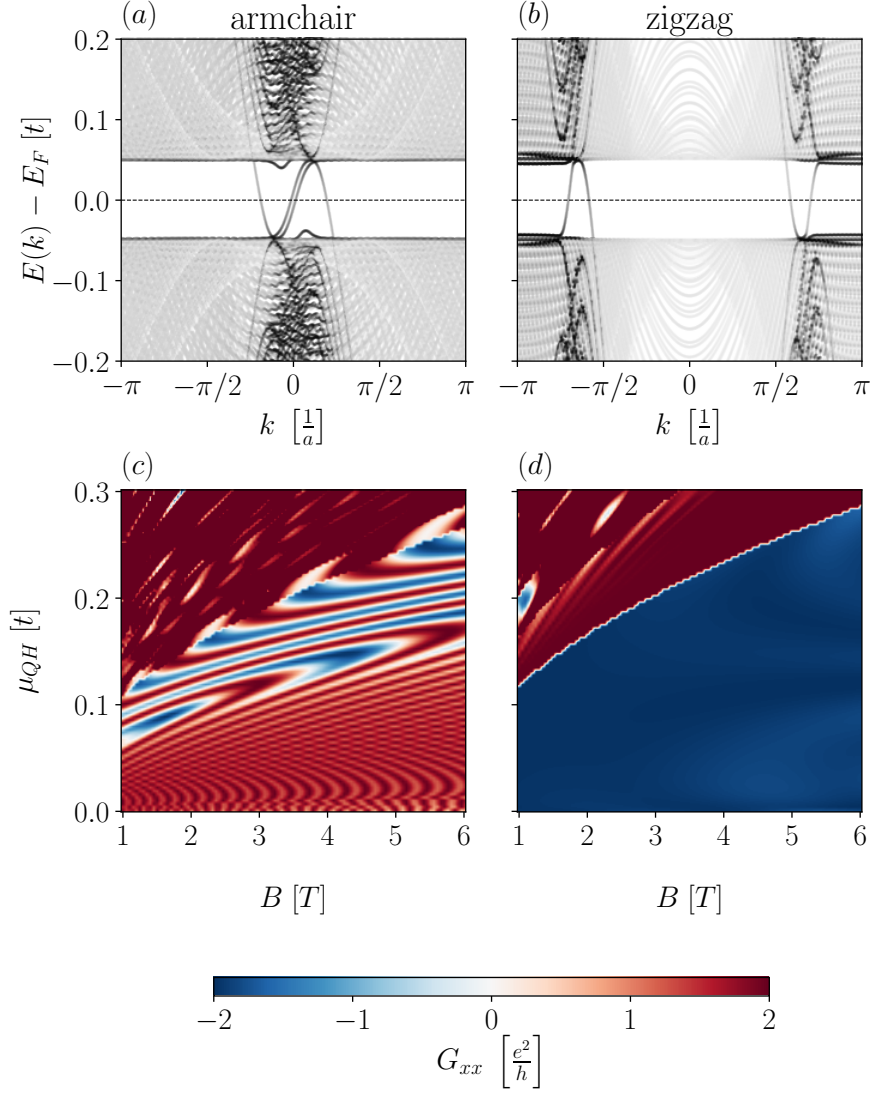


Figure 2: Band structure of a NS ribbon with (a) armchair and (b) zigzag terminations with $\mu_{QH} = \mu_{SC} = 0.05t$, $B = 1$ T. The opacity is the expectation value of $f(\mathbf{r}_i)$, defined in Eq. 5, with $\chi = 5$. We see that the positive velocity modes (chiral Andreev states) occur near $k = 0$ with armchair interfaces and are well-separated in momentum space for zigzag orientation. The resulting nonlocal conductance presents an interference pattern for armchair interfaces (c) while the expected constant value from Eq. 1 is obtained for zigzag interfaces (d).

edge states at the normal edge couple with the bands at the NS interface, including the additional non-chiral ones, valley conservation no longer constrains the conductance to the quantized value. In agreement with this expectation, including the doping by the superconductor in the numerical simulations produces an interference pattern in the nonlocal Andreev conductance, shown in Fig. 4(b). Naturally, interface disorder spoils this regular interference pattern due to the interface doping.

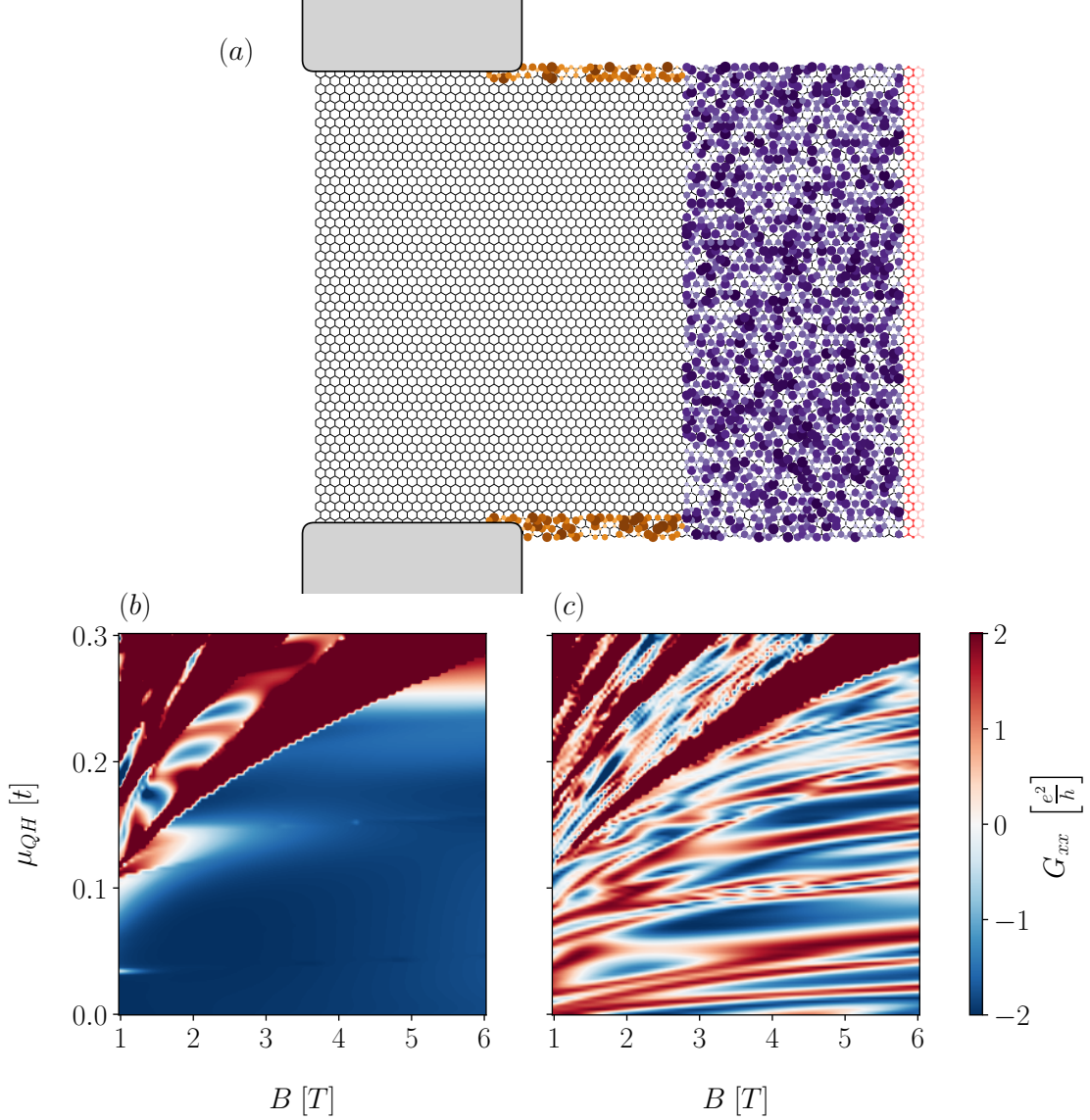


Figure 3: Effects of disorder on the downstream resistance. (a) Scheme of disorder landscape: orange represents $\delta\mu_i^{(\text{edge})}$; purple represents $\delta\mu_i^{(\text{SC})}$. The resulting nonlocal conductance with finite $\delta\mu_i^{(\text{edge})}$ (b) is minor and the conductance is still nearly constant in a large area of the parameter space. When $\delta\mu_i^{(\text{SC})}$ is finite (c), however, the effects are much stronger and persistent for all μ and B . The other parameters are chosen to be the same as in Fig. 2.

5 Experimental relevance

Comparing the alternative mechanisms, we observe that irregular oscillations, similar to the ones observed experiment, only arise due to the NS interface disorder. Thus, irregular sign changes in nonlocal transport measurements are an indication of a disordered NS interface. On the other hand, devices with a clean NS interface, are expected to have a conductance that is

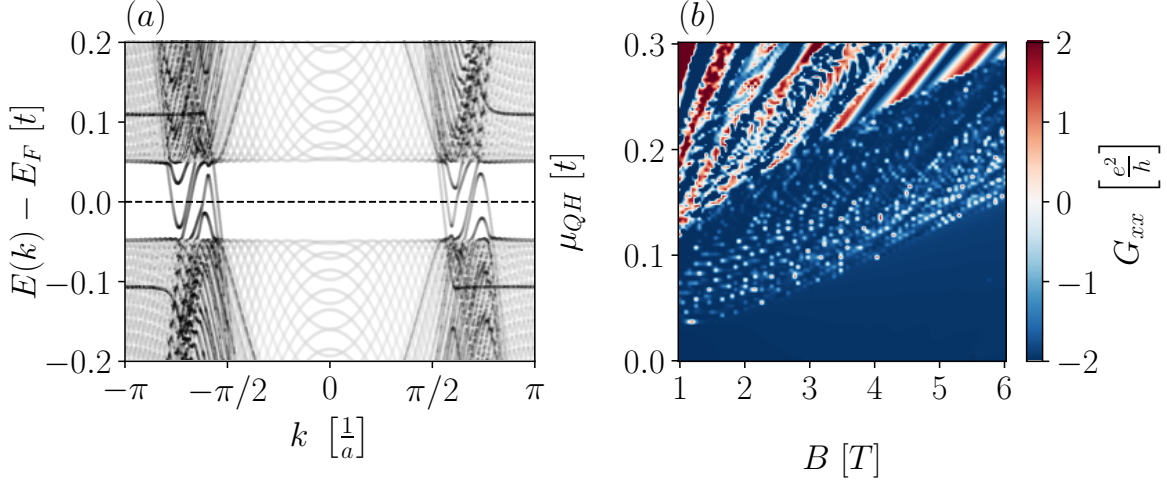


Figure 4: (a) Band structure of a NS ribbon with Fermi energy mismatch ($\mu_{QH} = 0.1t$, $\mu_{SC} = 0.5t$, and $B = 1$ T). The opacity is the same as in Fig. 2. One can clearly see the presence of extra non-chiral edge states. (b) Nonlocal conductance of a system with finite Fermi level mismatch ($\mu_{SC} = 0.5t$). There is a clear deviation from the predicted constant value of Eq. 1 due to the extra propagating modes.

either nearly constant or that exhibits regular oscillations caused by the Fermi level mismatch. While our analysis disregarded the effect of Bogoliubov vortices, we expect that these act as quasiparticle sinks and lower the overall magnitude of the nonlocal conductance, similar to what is observed in Ref. [16] (see the detailed discussion in App. C).

Recent experimental works [15–17] motivate the combination of quantum Hall effect and superconducting order in graphene as a platform for Majorana zero modes [28]. Our results cover two different situations that prevent the existence of a non-trivial topological phase: (i) the strong intervalley scattering caused by disorder closes the topological gap; (ii) Fermi level mismatch promotes the population of undesired edge states along the NS interface [28, 29]. Therefore, there is a need to fabricate high-quality graphene/superconductor heterostructures, *e.g.*, substituting the current superconductor deposition techniques by stacking van der Waals materials, such as NbSe₂ [26]. Moreover, future works would benefit from electrostatic simulations to properly analyze the edge states population at the NS interface. Alternatively, experiments should explore routes to suppress the Fermi level mismatch.

6 Conclusion

We analysed three mechanisms responsible for fluctuations of Andreev conductance in quantum Hall graphene devices. We concluded that a clean NS interface couples edge states from different valleys only if it is precisely aligned with the armchair direction—an unlikely occurrence in experimental devices. Turning to imperfect interfaces, we observed that short-range disorder enables scattering between the two edge states with opposite valley polarizations, leading to irregular Andreev conductance oscillations that resemble the experimental data [16]. Finally,

we found that, even if the NS interface is clean, the Fermi level mismatch populates non-chiral edge states along the NS interface and therefore leads to Andreev conductance oscillations. We believe that our analysis of the Andreev edge state scattering mechanisms is exhaustive, and therefore it allows to qualitatively analyse the NS interface properties. Furthermore, we argue that the intense search for Majorana physics in graphene quantum Hall devices requires improvements in the NS interface quality and proper understanding and control of the Fermi level mismatch.

Acknowledgements

The authors thank Jose Lado and Kostas Vilkelis for useful discussions.

Author contributions A.R.A. formulated and supervised the project. A.L.R.M., I.M.F., and C.-X.L. performed numerical calculations and identified the possible causes of conductance oscillations. A.L.R.M. developed the analytical model. The authors wrote the manuscript jointly.

Funding information This work was supported by grants #2016/10167-8 and #2019/07082-9, São Paulo Research Foundation; by a subsidy for top consortia for knowledge and innovation (TKI toeslag) by the Dutch ministry of economic affairs; and by VIDI grants 680-47-537 and 016.Vidi.189.180.

Data availability

The code and data used to produce the figures and derive the effective model are available in Ref. [30]. We use Adaptive [31] to efficiently sample k -space for the band structure calculations.

A Valley-dependence of Andreev reflection in quantum Hall graphene

Andreev reflection is a process in which an incoming charge carrier reflects as its time-reversal partner. In graphene, it means that electrons convert to holes in the opposite valley [6, 27]. Thus, charge and valley densities are correlated. Moreover, boundary conditions applied to graphene's lowest Landau level result in valley-polarized edge modes [21, 22]. We can observe both phenomena by computing the local values of valley and charge densities, as shown in Fig. 5. We compute the valley density as the expectation value of the anti-Haldane operator, V [32, 33]. In the presence of a magnetic field, we must include a Peierls phase $\phi_{ij}(B)$:

$$V(B) = \frac{i}{3\sqrt{3}} \sum_{\langle\langle i,j \rangle\rangle} \eta_{ij} s_z^{ij} e^{i\phi_{ij}(B)} c_i^\dagger c_j, \quad (9)$$

where $\langle\langle i,j \rangle\rangle$ denotes a sum performed over the next-nearest-neighbors, $\eta_{ij} = \pm 1$ for a clockwise/anticlockwise hopping, and $s_z = \pm 1$ if \mathbf{r}_i is in the A/B sublattice.

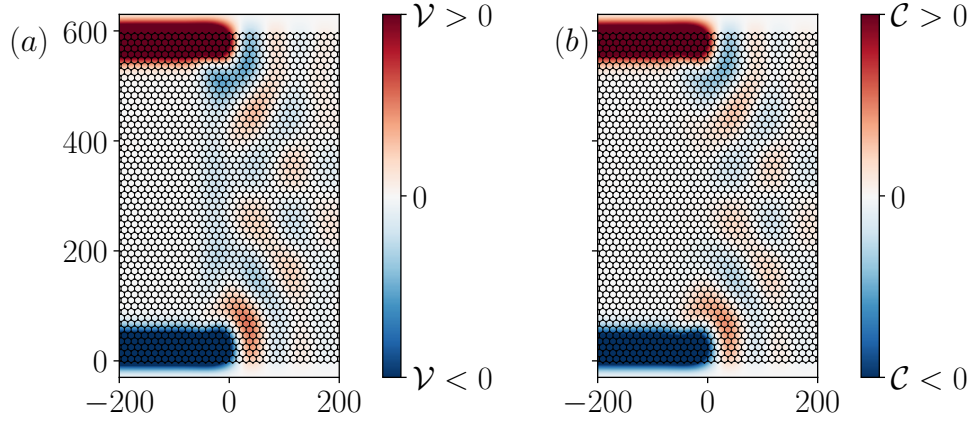


Figure 5: (a) Valley, $\mathcal{V}(\mathbf{r}) = \langle \mathbf{r} | V(B) | \mathbf{r} \rangle$, and (b) charge, $\mathcal{C}(\mathbf{r}) = \langle \mathbf{r} | -\tau_z | \mathbf{r} \rangle$, densities near a NS interface ($x = 0$) with $B = 1$ T and $\mu = 0.075t$. It is visible that both incoming and outgoing modes are valley polarized and that charge and valley densities are highly correlated. The length is in units of nm (the honeycomb crystal in the background is purely illustrative).

In a two-terminal setup with a NS interface, the longitudinal conductance in the lowest Landau level was previously shown to be [19]:

$$G_{NS} = \frac{2e^2}{h}(1 - \cos \Phi), \quad (10)$$

where Φ is the angle difference between the valley isospins of the states entering and leaving the superconductor, depicted in Fig. 6(a). It turns out that Φ depends on the geometry, resulting in constant conductance with different values, as shown in Fig. 6(b).

It is straightforward to compute the nonlocal conductance G_{xx} of a 3-terminal device as the one depicted in Fig. 1. First, we take $\Phi = \pi$. Then, we notice that

$$G_{xx} = \frac{2e^2}{h} - G_{NS} = \frac{2e^2}{h} \cos \Phi, \quad (11)$$

leading to Eq. 1.

B Low-energy model derivation

To derive the low-energy effective model presented in Sec. 2, we start with the valley-symmetric Dirac-Bogoliubov-de Gennes Hamiltonian [21] version of Eq. 4 for an infinite system along the y -axis. We also take $\chi \rightarrow 0$, such that $f(\mathbf{r}_i) \rightarrow \Theta(\mathbf{r}_i)$. The Hamiltonian reads

$$H = \hbar v \tau_z \otimes [-i \rho_0 \sigma_x \partial_x + (k \rho_0 + k_0 \rho_z) \otimes \sigma_y] - \mu \tau_z \otimes \rho_0 \otimes \sigma_0 + \tau_0 \otimes \rho_0 \otimes v \mathbf{A}(x) \cdot \sigma + \Delta(x) \tau_x \otimes \rho_0 \otimes \sigma_0, \quad (12)$$

where the ρ and s Pauli matrices act on valley and sublattice spaces, k is the momentum along the y -direction, and k_0 is the Dirac nodes momentum for an arbitrary nanoribbon orientation.

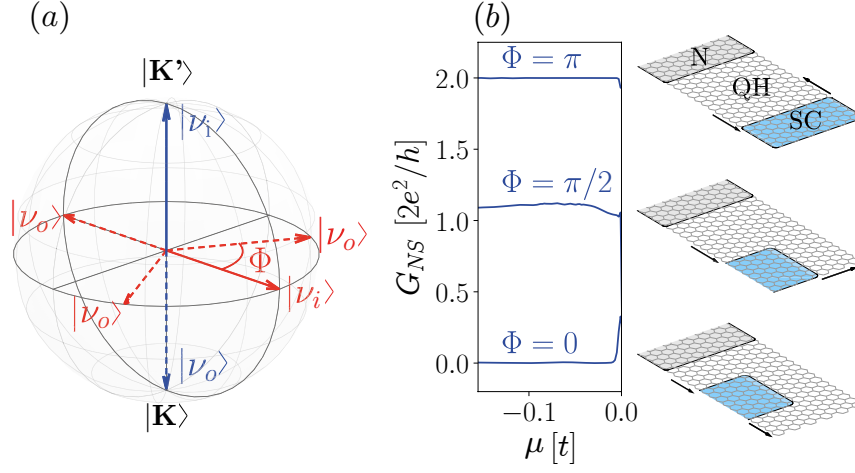


Figure 6: (a) Incoming ν_i (solid) and outgoing ν_o (dashed) valley isospins on the Bloch sphere. Modes propagating along a zigzag boundary are valley polarized (blue) whereas in an armchair interfaces they are composed by a linear combination of both valley states. (b) G_{NS} conductance plateaus from setups with different arrangements of the superconductor on a NS junction. The angle difference Φ between the valley isospin of incoming and outgoing modes depends only on the device geometry.

We also simplify the problem by taking μ to be constant over the entire system.

We now compute the effective Hamiltonian using first order in perturbation theory [28,29,34]. The perturbation is

$$H_{\text{pert}} = \hbar v (k\rho_0 + k_0\rho_z) \otimes \sigma_y, \quad (13)$$

and the unperturbed term is

$$H_0 = H - H_{\text{pert}}. \quad (14)$$

Thus, the effective Hamiltonian is obtained by computing

$$(H_{\text{eff}})_{ij} := \langle \psi_i | H_{\text{pert}} | \psi_j \rangle, \quad (15)$$

where $\{\psi_i\}$ are the zero-energy solutions of H_0 .

In order to find $\{\psi_i\}$, we solve

$$\partial_x \psi = m(x) \psi, \quad (16)$$

$$m(x) = \frac{i\Gamma_1^{-1}}{\hbar v} [eBx\Theta(x)\Gamma_4 + \mu\Gamma_0 - \Delta\Theta(x)\Gamma_3], \quad (17)$$

where we used Γ -matrices defined as:

$$\Gamma_0 := \tau_z \otimes \rho_0 \otimes \sigma_0, \quad (18)$$

$$\Gamma_1 := \tau_z \otimes \rho_0 \otimes \sigma_x, \quad (19)$$

$$\Gamma_2 := \tau_z \otimes \rho_0 \otimes \sigma_y, \quad (20)$$

$$\Gamma_3 := \tau_x \otimes \rho_0 \otimes \sigma_0, \quad (21)$$

$$\Gamma_4 := \tau_0 \otimes \rho_0 \otimes \sigma_y, \quad (22)$$

$$\Gamma_5 := \tau_z \otimes \rho_z \otimes \sigma_y. \quad (23)$$

Thus,

$$\psi(x) = \psi_i(x) e^{\lambda_i(x)}, \quad (24)$$

where $\psi_\alpha(x)$ and $\lambda_\alpha(x)$ are the eigenvectors and eigenvalues of

$$M(x) = \int_0^x d\xi \, m(\xi). \quad (25)$$

We then have

$$\psi_i = \frac{1}{\mathcal{N}} \left(\psi_i^{x<0} \Theta(-x) + \psi_i^{x>0} \Theta(x) \right), \quad i = 1, 2, \quad (26)$$

where \mathcal{N} is the normalization constant,

$$\psi_1^{x<0} = \begin{pmatrix} g(x) \\ i \\ 0 \\ 0 \\ ig(x) \\ 1 \\ 0 \\ 0 \end{pmatrix} \alpha(x), \quad \psi_1^{x>0} = \begin{pmatrix} i \\ i \\ 0 \\ 0 \\ 1 \\ 1 \\ 0 \\ 0 \end{pmatrix} \beta(x), \quad (27)$$

and

$$\psi_2^{x<0} = \begin{pmatrix} 0 \\ 0 \\ g(x) \\ i \\ 0 \\ 0 \\ 0 \\ i \\ g(x) \end{pmatrix} \alpha(x), \quad \psi_2^{x>0} = \begin{pmatrix} 0 \\ 0 \\ i \\ i \\ 0 \\ 0 \\ 0 \\ 1 \\ 1 \end{pmatrix} \beta(x), \quad (28)$$

with

$$g(x) = -\frac{2\mu x}{Bex^2 - 2(B^2 e^2 x^2/4 - \mu^2)^{1/2} |x|}, \quad (29)$$

$$\alpha(x) = e^{-\frac{(B^2 e^2 x^2/4 - \mu^2)^{1/2} |x|}{\hbar v_F}}, \quad (30)$$

$$\beta(x) = e^{-\frac{x(\Delta - i\mu)}{\hbar v_F}}. \quad (31)$$

It is easy to see that ψ_1 is a linear combination of an electron state at the valley K with a hole state at valley K' , while ψ_2 is the opposite. Using Eq. 15, it is straightforward to obtain Eq. 2. Finally, the intervalley scattering term from Eq. 3 is obtained by adding $\omega\tau_0 \otimes \rho_x \otimes \sigma_0$ to Eq. 13.

C Absorption of quasi-particle excitations by the superconductor

The quasiparticles absorption by the superconductor reduces the probability of outgoing electrons and holes at the end of the interface. We effectively add a “survival probability” P_{surv} by modifying the system: we attach a metallic lead to the superconducting region such that quasiparticles can now tunnel through the superconductor with a finite probability. Thus, the nonlocal conductance change as [16]

$$\tilde{G}_{xx} = P_{\text{surv}} G_{xx} \quad (32)$$

where G_{xx} is given by Eq. 11. Thus, the nonlocal conductance is suppressed, as seen in (Fig. 7, following experimental results [16]).

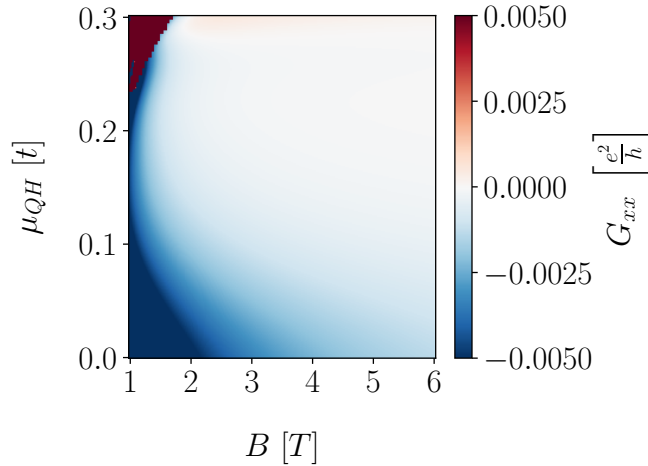


Figure 7: (a) Quasiparticle tunneling to the superconductor suppresses the nonlocal conductance. We choose the same parameters as the ones used in Fig. 2 but with a metallic lead ($\Delta = 0$) connected to the superconductor in the scattering region.

References

- [1] H. B. Heersche, P. Jarillo-Herrero, J. B. Oostinga, L. M. Vandersypen and A. F. Morpurgo, *Induced superconductivity in graphene*, Solid State Communications **143**(1), 72 (2007), doi:<https://doi.org/10.1016/j.ssc.2007.02.044>, Exploring graphene.

- [2] H. B. Heersche, P. Jarillo-Herrero, J. B. Oostinga, L. M. K. Vandersypen and A. F. Morpurgo, *Bipolar supercurrent in graphene*, Nature **446**(7131), 56 (2007), doi:[10.1038/nature05555](https://doi.org/10.1038/nature05555).
- [3] J. I.-J. Wang, L. Bretheau, D. Rodan-Legrain, R. Pisoni, K. Watanabe, T. Taniguchi and P. Jarillo-Herrero, *Tunneling spectroscopy of graphene nanodevices coupled to large-gap superconductors*, Phys. Rev. B **98**, 121411 (2018), doi:[10.1103/PhysRevB.98.121411](https://doi.org/10.1103/PhysRevB.98.121411).
- [4] J.-B. Qiao, Y. Gong, W.-J. Zuo, Y.-C. Wei, D.-L. Ma, H. Yang, N. Yang, K.-Y. Qiao, J.-A. Shi, L. Gu and L. He, *One-step synthesis of van der waals heterostructures of graphene and two-dimensional superconducting α -Mo₂C*, Phys. Rev. B **95**, 201403 (2017), doi:[10.1103/PhysRevB.95.201403](https://doi.org/10.1103/PhysRevB.95.201403).
- [5] V. E. Calado, S. Goswami, G. Nanda, M. Diez, A. R. Akhmerov, K. Watanabe, T. Taniguchi, T. M. Klapwijk and L. M. K. Vandersypen, *Ballistic Josephson junctions in edge-contacted graphene*, Nature Nanotechnology **10**(9), 761 (2015), doi:[10.1038/nnano.2015.156](https://doi.org/10.1038/nnano.2015.156).
- [6] M. Titov and C. W. J. Beenakker, *Josephson effect in ballistic graphene*, Phys. Rev. B **74**, 041401 (2006), doi:[10.1103/PhysRevB.74.041401](https://doi.org/10.1103/PhysRevB.74.041401).
- [7] C. T. Ke, A. W. Draelos, A. Seredinski, M. T. Wei, H. Li, M. Hernandez-Rivera, K. Watanabe, T. Taniguchi, M. Yamamoto, S. Tarucha, Y. Bomze, I. V. Borzenets *et al.*, *Anomalous periodicity of magnetic interference patterns in encapsulated graphene josephson junctions*, Phys. Rev. Research **1**, 033084 (2019), doi:[10.1103/PhysRevResearch.1.033084](https://doi.org/10.1103/PhysRevResearch.1.033084).
- [8] X. Du, I. Skachko and E. Y. Andrei, *Josephson current and multiple andreev reflections in graphene sns junctions*, Phys. Rev. B **77**, 184507 (2008), doi:[10.1103/PhysRevB.77.184507](https://doi.org/10.1103/PhysRevB.77.184507).
- [9] S. Bhandari, G.-H. Lee, K. Watanabe, T. Taniguchi, P. Kim and R. M. Westervelt, *Imaging andreev reflection in graphene*, Nano Letters **20**(7), 4890 (2020), doi:[10.1021/acs.nanolett.0c00903](https://doi.org/10.1021/acs.nanolett.0c00903).
- [10] B. M. Kessler, i. m. c. O. Girit, A. Zettl and V. Bouchiat, *Tunable superconducting phase transition in metal-decorated graphene sheets*, Phys. Rev. Lett. **104**, 047001 (2010), doi:[10.1103/PhysRevLett.104.047001](https://doi.org/10.1103/PhysRevLett.104.047001).
- [11] A. Allain, Z. Han and V. Bouchiat, *Electrical control of the superconducting-to-insulating transition in graphene-metal hybrids*, Nature Materials **11**(7), 590 (2012), doi:[10.1038/nmat3335](https://doi.org/10.1038/nmat3335).
- [12] M. Popinciuc, V. E. Calado, X. L. Liu, A. R. Akhmerov, T. M. Klapwijk and L. M. K. Vandersypen, *Zero-bias conductance peak and josephson effect in graphene-nbtin junctions*, Phys. Rev. B **85**, 205404 (2012), doi:[10.1103/PhysRevB.85.205404](https://doi.org/10.1103/PhysRevB.85.205404).
- [13] F. E. Schmidt, M. D. Jenkins, K. Watanabe, T. Taniguchi and G. A. Steele, *A ballistic graphene superconducting microwave circuit*, Nature Communications **9**(1), 4069 (2018), doi:[10.1038/s41467-018-06595-2](https://doi.org/10.1038/s41467-018-06595-2).
- [14] G.-H. Lee, D. K. Efetov, W. Jung, L. Ranzani, E. D. Walsh, T. A. Ohki, T. Taniguchi, K. Watanabe, P. Kim, D. Englund and K. C. Fong, *Graphene-based josephson junction microwave bolometer*, Nature **586**(7827), 42 (2020), doi:[10.1038/s41586-020-2752-4](https://doi.org/10.1038/s41586-020-2752-4).

- [15] G.-H. Lee, K.-F. Huang, D. K. Efetov, D. S. Wei, S. Hart, T. Taniguchi, K. Watanabe, A. Yacoby and P. Kim, *Inducing superconducting correlation in quantum Hall edge states*, Nature Physics **13**(7), 693 (2017), doi:[10.1038/nphys4084](https://doi.org/10.1038/nphys4084).
- [16] L. Zhao, E. G. Arnault, A. Bondarev, A. Seredinski, T. F. Larson, A. W. Draelos, H. Li, K. Watanabe, T. Taniguchi, F. Amet *et al.*, *Interference of chiral Andreev edge states / Nature Physics*, <https://www.nature.com/articles/s41567-020-0898-5> (2020).
- [17] Önder Gül, Y. Ronen, S. Y. Lee, H. Shapourian, J. Zauberman, Y. H. Lee, K. Watanabe, T. Taniguchi, A. Vishwanath, A. Yacoby and P. Kim, *Induced superconductivity in the fractional quantum hall edge* (2020), [2009.07836](https://doi.org/2009.07836).
- [18] G.-H. Park, M. Kim, K. Watanabe, T. Taniguchi and H.-J. Lee, *Propagation of superconducting coherence via chiral quantum-Hall edge channels*, Scientific Reports **7**(1), 10953 (2017), doi:[10.1038/s41598-017-11209-w](https://doi.org/10.1038/s41598-017-11209-w).
- [19] A. R. Akhmerov and C. W. J. Beenakker, *Detection of Valley Polarization in Graphene by a Superconducting Contact*, Physical Review Letters **98**(15), 157003 (2007), doi:[10.1103/PhysRevLett.98.157003](https://doi.org/10.1103/PhysRevLett.98.157003).
- [20] L. Brey and H. A. Fertig, *Edge states and the quantized hall effect in graphene*, Phys. Rev. B **73**, 195408 (2006), doi:[10.1103/PhysRevB.73.195408](https://doi.org/10.1103/PhysRevB.73.195408).
- [21] A. R. Akhmerov and C. W. J. Beenakker, *Boundary conditions for Dirac fermions on a terminated honeycomb lattice*, Physical Review B **77**(8), 085423 (2008), doi:[10.1103/PhysRevB.77.085423](https://doi.org/10.1103/PhysRevB.77.085423).
- [22] M. O. Goerbig, *Electronic properties of graphene in a strong magnetic field*, Reviews of Modern Physics **83**(4), 1193 (2011), doi:[10.1103/RevModPhys.83.1193](https://doi.org/10.1103/RevModPhys.83.1193).
- [23] C. W. Groth, M. Wimmer, A. R. Akhmerov and X. Waintal, *Kwant: A software package for quantum transport*, New Journal of Physics **16**(6), 063065 (2014), doi:[10.1088/1367-2630/16/6/063065](https://doi.org/10.1088/1367-2630/16/6/063065).
- [24] M.-H. Liu, P. Rickhaus, P. Makk, E. Tóvári, R. Maurand, F. Tkatschenko, M. Weiss, C. Schönenberger and K. Richter, *Scalable Tight-Binding Model for Graphene*, Physical Review Letters **114**(3), 036601 (2015), doi:[10.1103/PhysRevLett.114.036601](https://doi.org/10.1103/PhysRevLett.114.036601).
- [25] A. H. Castro Neto, F. Guinea, N. M. R. Peres, K. S. Novoselov and A. K. Geim, *The electronic properties of graphene*, Rev. Mod. Phys. **81**, 109 (2009), doi:[10.1103/RevModPhys.81.109](https://doi.org/10.1103/RevModPhys.81.109).
- [26] J. Li, H.-B. Leng, H. Fu, K. Watanabe, T. Taniguchi, X. Liu, C.-X. Liu and J. Zhu, *Superconducting proximity effect in a transparent van der Waals superconductor-metal junction*, Physical Review B **101**(19), 195405 (2020), doi:[10.1103/PhysRevB.101.195405](https://doi.org/10.1103/PhysRevB.101.195405), [2005.02314](https://arxiv.org/abs/2005.02314).
- [27] C. W. J. Beenakker, *Specular andreev reflection in graphene*, Phys. Rev. Lett. **97**, 067007 (2006), doi:[10.1103/PhysRevLett.97.067007](https://doi.org/10.1103/PhysRevLett.97.067007).

- [28] P. San-Jose, J. L. Lado, R. Aguado, F. Guinea and J. Fernández-Rossier, *Majorana Zero Modes in Graphene*, Physical Review X **5**(4), 041042 (2015), doi:[10.1103/PhysRevX.5.041042](https://doi.org/10.1103/PhysRevX.5.041042).
- [29] A. L. R. Manesco, G. Weber and D. Rodrigues, *Effective model for majorana modes in graphene*, Phys. Rev. B **100**, 125411 (2019), doi:[10.1103/PhysRevB.100.125411](https://doi.org/10.1103/PhysRevB.100.125411).
- [30] A. L. R. Manesco, I. M. Flór, C.-X. Liu and A. R. Akhmerov, *Mechanisms of Andreev reflection in quantum Hall graphene*, doi:[10.5281/zenodo.4597080](https://doi.org/10.5281/zenodo.4597080) (2021).
- [31] B. Nijholt, J. Weston, J. Hoofwijk and A. Akhmerov, *Adaptive: parallel active learning of mathematical functions*, doi:[10.5281/zenodo.1182437](https://doi.org/10.5281/zenodo.1182437) (2019).
- [32] E. Colomés and M. Franz, *Antichiral edge states in a modified haldane nanoribbon*, Phys. Rev. Lett. **120**, 086603 (2018), doi:[10.1103/PhysRevLett.120.086603](https://doi.org/10.1103/PhysRevLett.120.086603).
- [33] A. Ramires and J. L. Lado, *Electrically tunable gauge fields in tiny-angle twisted bilayer graphene*, Phys. Rev. Lett. **121**, 146801 (2018), doi:[10.1103/PhysRevLett.121.146801](https://doi.org/10.1103/PhysRevLett.121.146801).
- [34] J. L. Lado and M. Sigrist, *Two-dimensional topological superconductivity with antiferromagnetic insulators*, Phys. Rev. Lett. **121**, 037002 (2018), doi:[10.1103/PhysRevLett.121.037002](https://doi.org/10.1103/PhysRevLett.121.037002).